JOURNAL OF MATERIALS SCIENCE 10 (1975) 1519–1526

The plastic deformation of copper–2 at. % cobalt alloy single crystals

KAMAL E. AMIN,* VOLKMAR GEROLD, GERHARD KRALIK
Max-Planck-Institut für Metallforschung, Institut für Werkstoffwissenschaften, und Institut für Metallkunde, Universität Stuttgart, Stuttgart, Germany

Copper–2 at. % cobalt alloy single crystals containing coherent and/or incoherent spherical cobalt precipitates (60 Å < R < 420 Å) have been tested in tension at 77 and 295 K. The precipitation process and the dislocation substructure were examined by electron microscopy. The yielding process is consistent with the Orowan mechanism, and the work-hardening of the alloy is parabolic in nature for small and medium size particles but changes to three-stage hardening for larger particles. The extent of stage I deformation is temperature dependent, and the rate of work-hardening is steep and may be described by either the Ashby or the Hirsch parabolic hardening models. There is a noticeable softening during this stage which may be attributable to shearing of the particles during deformation. The dislocation substructure shows typical jogged screw dislocations as well as a few loops and dipoles, and the precipitates are a mixture of semi-coherent and incoherent particles. Transformation to incoherent particles is enhanced by deformation, and the secondary stage hardening rate increases with the size of cobalt particle but is independent of temperature.

1. Introduction

Second phase precipitates in a metallic matrix act as a barrier to the movement of dislocations, forcing them to behave in one of two ways: either to cut through the particles or to take a circuitous path around the obstacles. Coherent precipitates of fcc cobalt with radii below about 100 Å in copper–cobalt single crystals [1], as well as γ-iron precipitates in copper–iron [2], were reported previously to have been cut during plastic deformation. After not too long ageing times, stage I in copper–cobalt becomes longer and steeper, whilst in copper–iron it becomes shorter. A negative curvature of this stage I is attributed to the shearing of particles. Particle shearing was also reported in polycrystalline copper–cobalt alloys [3, 4].

On the other hand, copper alloys containing large particles of SiO_2, BeO or Al_2O_3 [5-10], as well as overaged Al–Cu alloys [11], show quite a different behaviour. Their flow curves are quasi-parabolic with very large initial hardening rates. Since the precipitates are non-deformable, the yield stress is controlled by the Orowan mechanism, and the work-hardening rate is interpreted by the interaction of primary dislocations and geometrically necessary dislocations. The geometrically necessary dislocations, as defined by Ashby [12], are those formed at the non-deforming particle interfaces by cross slip, secondary slip and prismatic punching to accommodate the different deformation of the particle and matrix. The electron microscopy of these crystals as deformed in stage I shows [8-10] rows of prismatic loops, helices, a large density of dipoles and many secondary dislocations generated at the particles, whilst in the case of coherent particles the majority of the dislocations are primary [13].

The precipitation process in Cu–Co, with and without prior deformation, has been studied previously by Phillips [14, 15]. Electron microscopic observations on the kinetics of precipitation in undeformed Cu–3.1 wt % Co alloys suggested that the overageing process is a result of an increase in particle spacing, progressive loss of coherency and an increase in the amount of discontinuous precipitation. Loss of full coherency did not occur until well into the overaged region, even with the assistance of deformation after ageing. The experiments [16] indicated no critical size for peak hardening, contradicting

*Present address: Institut für Werkstoffwissenschaften I, Universität Erlangen-Nürnberg, Germany.

earlier observations [3]. Humphreys [17] has found that cobalt particles up to a size of about 120 Å radius remain coherent after deformation and are sheared with the matrix, while particles above about 170 Å radius lose coherency during deformation. He suggested that dislocations by-pass some of these particles by cross slip while the majority are being sheared. Earlier work by Gleiter [5] had suggested a combination of cross slip and shear in this range too.

The above-mentioned findings have led to the present work for which a copper–2 at. % cobalt alloy was chosen. Single crystals were given a suitable heat-treatment yielding a wide range of cobalt-rich solid-solution precipitate sizes in the underaged, aged and overaged states. The main purpose was to study the yielding and work-hardening of the alloy single crystals having an orientation near the centre of the standard triangle as a function of particle size, to understand the ageing process and the effect of deformation on coherency transformation, and finally to check the validity of some models in describing the age-hardening process.

2. Experimental procedure

The copper–2 at. % cobalt alloy was prepared by melting and casting in high vacuum from 99.99% copper and 99.8% cobalt. It was swaged to 4 mm diameter rods which were subsequently used to grow seeded single crystals using a modification of the Bridgeman technique. After checking the orientation, the samples were homogenized at 1000° C for 20 h, then fast-quenched into an ice-brine solution. Some samples were homogenized by thermal cycling ten times between 940 and 1030° C, each cycle lasting for 40 min, then quenched from 1030° C. The precipitation treatment was done under argon for various times ranging from $\frac{1}{2}$ h to 5 days in the temperature range 600 to 750° C. The crystals were later machined into tensile specimens of 20 mm gauge length either by spark erosion or by electrochemical thinning; in all cases the last treatment was electropolishing down to 3 mm diameter in a mixture of 1 vol HNO_3 and 2 vol CH_3OH. Tensile tests were carried out using an ordinary testing machine (Zwick) at 77 and 295 K and a strain-rate of 5.0×10^{-4} sec^{-1}. Samples for electron microscopy were prepared by spark cutting followed by jet polishing at − 40° C, using 13 to 15 V and the electrolyte mentioned above.

3. Experimental results and discussion

3.1. Electron microscopy

The coherent fcc cobalt-rich particles in the present alloy were visible due to diffraction contrast effects associated with the strain field around the particles. Incoherent particles were clearly visible due to absorption and orientation contrast difference relative to the matrix. In the latter case, the particles were seen to be nearly spherical in shape. Some of the precipitates were selectively etched away during thinning leaving "white" holes. The nature of these particles has been discussed in detail earlier by Phillips [14, 15]. The sizes were determined from the particles visible in the electron micrographs while their volume fraction was obtained from the equilibrium phase diagram [18]. Three separate estimates were carried out using Equations 1 and 2 below and by measuring directly and averaging the diameters of a few hundred particles in different regions of the foils after tilting to get the maximum visible particle density. The first equation [19] gives the particle radius (R) from the foil thickness (t), the number of particles per unit area (N_a) and the volume fraction (f_v)

$$R = \left(\frac{3tf_v}{4\pi N_a}\right)^{1/3}, \qquad (1)$$

and the second equation uses the number of particle intercepts per unit length (N_l)

$$R = (N_l/4N_a)\,. \qquad (2)$$

The estimates used for subsequent calculations are reported in Table I and plotted in Fig. 1 as particle radius versus precipitation time. In all

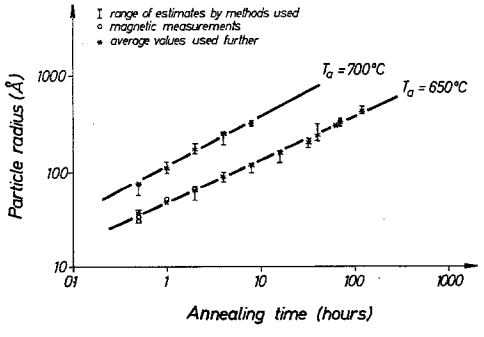

Figure 1 Particle growth in Cu–2 at. % Co at different temperatures. Open circles are magnetic measurements obtained by Becker [20].

estimates, a foil thickness of 3000 Å was used. For particle radii less than about 80 Å, previously

TABLE I

Heat-treatment			Particle radius (Å)	$\Delta\tau_0$ (kgf mm^{-2})		$10^2\theta_{II}/\mu$ (kgf mm^{-2})	
T_a (°C)	kf	t_a (h)		T_m = 77 K	T_m = 293 K	T_m = 77 K μ = 4400	T_m = 293 K μ = 4100
650	0.016	0.5	35	2.96	3.77	—	—
		1	48	4.27	4.24	—	—
		2	65	5.69	6.29	—	—
		4	90	5.0	5.61	—	1.05
		8	120	4.36	4.10	—	1.28
		16	160	3.75	4.50	1.20	1.65
		32	200	3.40	3.44	2.24	2.22
		40	240	3.10	—	1.97	—
		64	300	2.50	2.0	2.00	2.23
		70	330	2.45	—	2.42	—
		120	420	1.35	—	2.52	—
700	0.0124	0.5	75	4.04	2.92	—	1.40
		1	110	4.56	4.59	1.78	1.45
		2	170	3.30	3.30	1.72	2.42
		4	250	2.70	3.30	1.59	1.71
		8	320	2.40	3.10	3.3	2.43
750	0.009	1	170	2.86	—	1.56	—
600	0.089	30	—	—	—	1.50	—
		50	160	4.7	—	1.65	—

reported magnetic measurements [20] for the same alloy composition and heat-treatment have been included and reasonable agreement with these measurements is found.

Ageing up to 16 h at 650° C gives particles still mostly coherent (Fig. 2a). Incoherent particles start to form at longer annealing times at radii above about 160 Å (Fig. 2b). The micrographs show no further evidence for coherency after 70 h treatment at 650° C (Fig. 2c) where $R \approx 330$ Å, in agreement with the size range of transformation reported by Phillips [15]. It is to be noted that in the present work those particles which showed no strain-field contrast (bean-type contrast) were considered incoherent. Livingston's [3] idea that overageing is principally due to the spontaneous loss of coherency when particles reach the critical diameter appears to be invalid based on the present observations. In the present work, peak-hardening corresponds to a size $R \simeq 100$ Å, and complete incoherency corresponds to a size some 2 to 3 times this value.

The transformation to the incoherent state occurs at smaller radii with the help of plastic deformation (Fig. 2d). One possible mechanism by which dislocations could help particles to lose coherency is by the creation of the necessary prismatic loops around the particles by cross slip [21]. Brown and Ham [21] have compared the self energy of two loops with the interaction energy of one of the loops with the particles and found that the total energy is lowered when $R \geqslant R_0 = 2\boldsymbol{b}/3 \mid \epsilon \mid$, where R_0 should be an upper limit and is termed a critical particle radius for transformation upon deformation and ϵ is the misfit caused by the solute atom. If one applies the same principle to the present alloy, one obtains a value of $R_0 \cong 110$ Å which is still smaller but in order of magnitude agreement with the experiment. The present results suggest a value of $R_0 \simeq 150$ Å for deformation-induced coherency loss.

3.2. Effect of ageing time and temperature on the critical resolved shear stress

Fig. 3a and b show semi-logarithmic plots of the critical resolved shear stress (CRSS) at the deformation temperatures 77 and 295 K as a function of ageing time. The data shown represent average values obtained from three tests at each time and temperature. These values are presented in Table I, along with the rates of second stage work-hardening. They show typical ageing and overageing phenomena resulting in

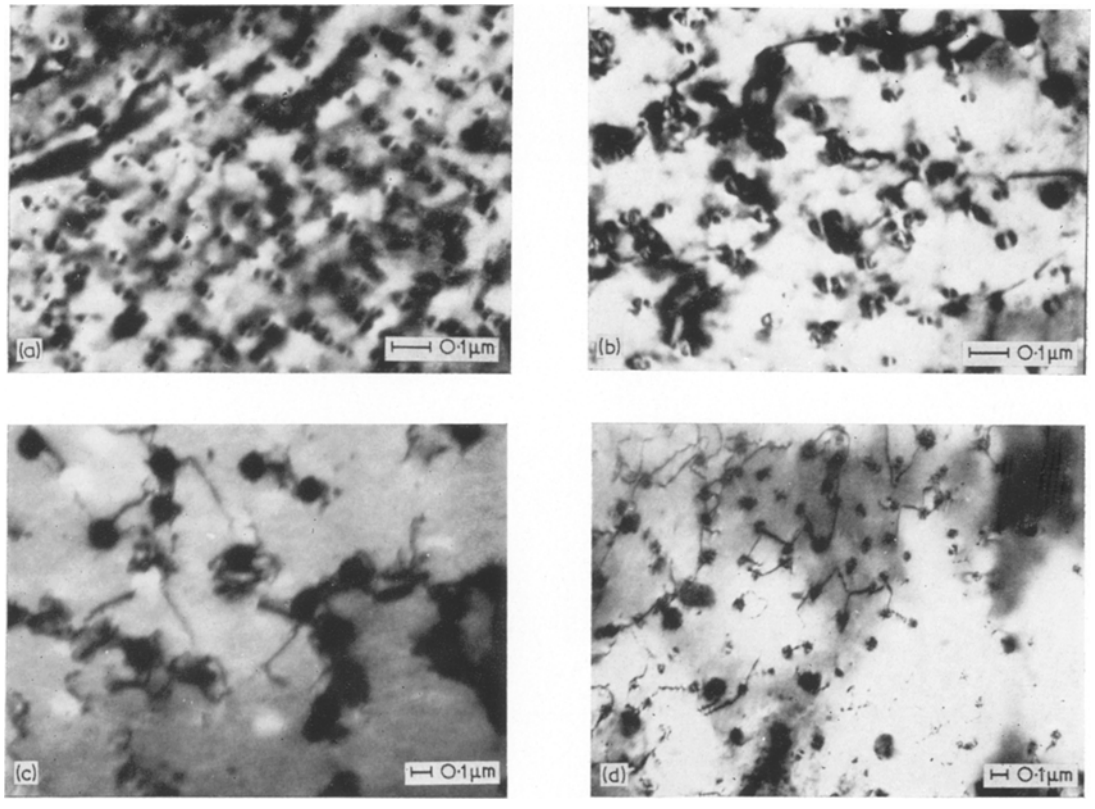

Figure 2 Transmission electron micrographs after different ageing treatments. (a) 8 h at 650°C, (b) 16 h at 650°C, (c) 70 h at 650°C, (d) 16 h at 650°C and slight deformation.

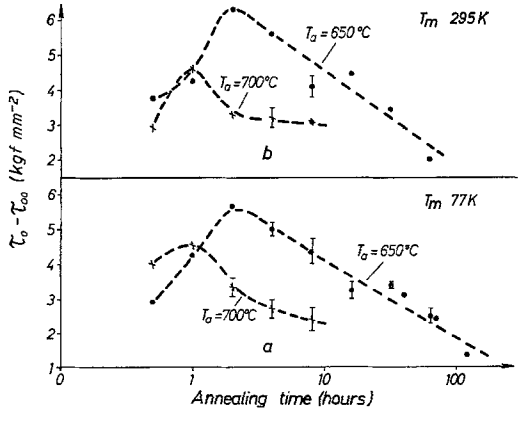

Figure 3 Increase of the CRSS at (a) 77 K and (b) 295 K as a function of the indicated annealing treatment.

a peak in the curve which increases in height with decreasing ageing temperature, probably due to decreased solubility of cobalt in copper. The so-called critical radius corresponding to maximum yield stress has a value of about 80 Å but varies with ageing and test temperature.

3.3. Tensile shear stress–shear strain curves

Fig. 4 shows some characteristic stress–strain curves for particle sizes from 90 to 330 Å radius and volume fractions ranging from 0.009 to 0.019. All experimental curves show a temperature-dependent first stage of quasi-parabolic work-hardening which extends up to about 70% shear strain. At particle sizes above 160 Å, this stage is less steep and is followed by a second stage, and the stress–strain curve becomes similar to that of a single phase crystal. Negligible serrations have been observed immediately following yielding for specimens aged for periods less than 16 h at 650°C, and in most cases the serrations did not go beyond 1 to 2% shear strain. Fig. 5 shows that the secondary stage hardening rate (θ_{II}) increases with particle size but is nearly independent of testing temperature and volume fraction of particles. This may

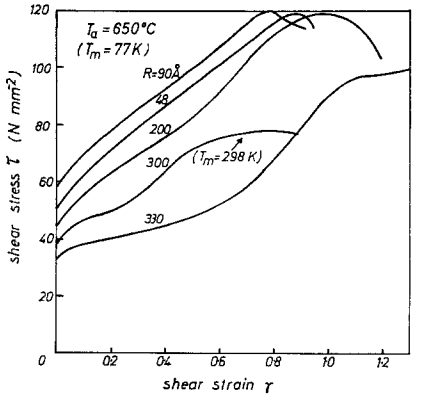

Figure 4 Representative shear stress–shear strain curves for Cu–Co single crystals; T_{in} = temperature of measurement, T_a = annealing temperature.

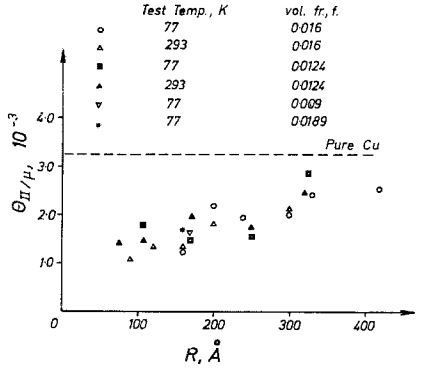

Figure 5 Dependence of stage II hardening rate on particle size.

be due to the influence of a higher dislocation density, both primary and secondary, formed near the large size particles and also to the fact that the smaller particles are more easily sheared during deformation.

3.4. Yielding

Since electron micrographs show the bean-type contrast for particle radii less than around 160 Å, it was deemed reasonable to analyse the data assuming coherency hardening. Previous treatments [21-25] for spherical particles lead to the equation:

$$\Delta\tau_0 = \alpha|\epsilon|^{3/2}\mu(fR/\boldsymbol{b})^{1/2}, \qquad (3)$$

where $\Delta\tau_0$ is the increase in critical shear stress, ϵ the distortion parameter expressed as the relative difference between the lattice constants of the precipitate and the matrix, R and f are the precipitate radius and volume fraction,

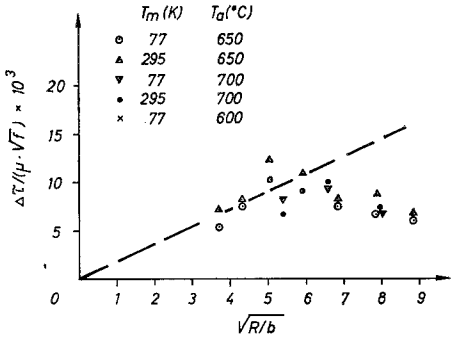

Figure 6 Normalized plot of yield stress versus square-root of particle size.

respectively, μ is the shear modulus and $\boldsymbol{b}$ the Burgers vector. α is a constant with a value of 3 to 4 [22]. The data plotted according to Equation 3 are presented in Fig. 6. In a previous work, Witt and Gerold [26] made similar experiments with single crystals, but mainly with smaller particles than in the present work. They found their data fitted a straight line up to $\sqrt{(R/\boldsymbol{b})} \simeq 5.3$ (R = 72 Å). It is this line that is indicated in Fig. 6 and shows that the data are consistent for the smaller particles.

Taking a misfit parameter $|\epsilon|$ value of 0.016, as expected from structural data, the experimental results yield a slope about one half of the value calculated from Equation 3. For particle sizes over about 100 Å, Equation 3 is no longer valid, as shown in Fig. 6, despite the fact that transmission electron micrographs clearly show the presence of coherency strains up to particle sizes of about 160 Å.

Since the critical shear stress drops again when the particle radius exceeds about 100 Å, the Orowan process is thought to operate at large particle sizes giving this inverse dependence on particle size. Ashby's formula [24, 25] for the Orowan mechanism was used in this analysis. It gives the increase in the critical resolved shear stress as

$$\Delta\tau_0 = 0.84\,\frac{2T}{\boldsymbol{b}(L - 1.6R)}, \qquad (4)$$

T is the line tension of the dislocation [6] in its critical position and is given by

$$T = \frac{\mu\boldsymbol{b}^2}{4\pi(1-\nu)^{1/2}}\ln(1.6\,R/r_0), \qquad (5)$$

where $\nu = 0.43$ is Poisson's ratio, r_0 is a lower cut-off radius for the dislocation strain field, and

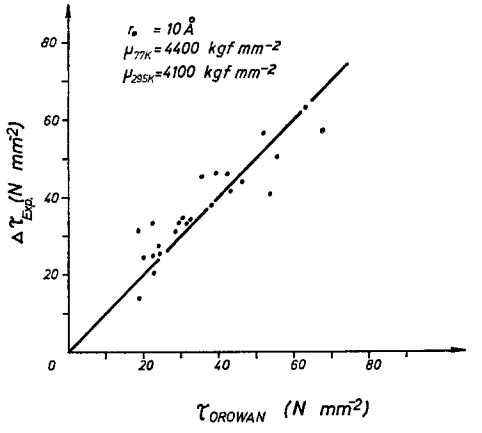

Figure 7 Experimental CRSS versus Orowan stress according to Equations 4 to 6 in the text.

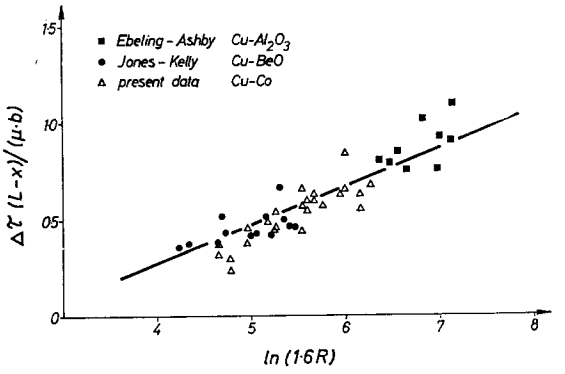

Figure 8 Normalized line tension versus particle radius comparing the values obtained on different dispersion hardening systems.

R is the precipitate radius. L is the effective particle spacing for a completely flexible dislocation:

$$L = \left(\frac{2}{f}\right)^{1/2} R \cdot \qquad (6)$$

Fig. 7 shows the values calculated from Equation 4 plotted against the experimental data. In order to obtain $\Delta\tau_0$ ($\Delta\tau_0 = \tau_0 - \tau_{00}$, where τ_{00} is the CRSS of the depleted matrix), the value for τ_{00} was estimated from a plot of τ_0 versus $c^{1/2}$ for crystals deformed in the solid solution state (c = solute concentration). From this plot τ_{00} was chosen for the composition of the depleted matrix according to the phase diagram [18].

Within the experimental scatter, all the present data can be approximated by Equations 4 and 5 in the range of particle radii between 80 and 420 Å by choosing the reasonable value of 10 Å for r_0. In addition, the present $\Delta\tau_0$ data, along with those from Cu–Al_2O_3 [24] and Cu–BeO [27, 28], are plotted in Fig. 8 as $\Delta\tau_0(L - 1.6R)/\mu b$ versus $\ln(1.6R)$. According to Equations 4 and 5, a straight line should result from which the numerical factor in Equation 4 and the cut-off radius r_0 in Equation 5 can be evaluated. A best-fit straight line considering all the data gives a slope of 0.21 and an intercept $\ln r_0 = 2.8$ (r_0 = 16 Å). A similar plot, but without the present data, yields a slope of 0.20 and an intercept of 2.44 (r_0 = 11.5 Å) [29]. Considering the limited accuracy of the various data, all the results are, therefore, in reasonable agreement. Because of this agreement, one can conclude immediately from Fig. 8 that the data show the proper dependence on particle size, i.e. on the distance of neighbouring dislocation arms in the critical position for the Orowan process to operate.

3.5. Work-hardening and the parabolic range

It is generally agreed that strain-hardening in alloys with non-shearable particles is a consequence of the formation of Orowan or Hirsch loops at the dispersed particles. The high concentration of stress around the particles tends to induce relaxation processes. Ashby [6, 12] in his secondary slip theory assumed that the geometrically necessary dislocations formed by these processes control the work-hardening of the specimen. They contribute to work-hardening in two ways; individually by acting as obstacles to slip and collectively by creating a long-range back-stress with the wavelength equal to the particle spacing. His derivation gives the flow stress as:

$$\tau - \tau_0 = c'\mu(bf\gamma/R)^{1/2}, \qquad (9)$$

where $(\tau - \tau_0)$ is the increase in flow stress with strain γ. c' is a constant with a value of 0.14 to 0.29, and the other symbols have the usual meaning. Equation 9 is almost independent of the details of the dislocation model adopted. The precise mechanism by which secondary dislocations obstruct primary ones changes only the constant c'.

Equation 9 has been modified by Humphreys [8-10] based on the idea that the relaxation process can be described as a cross-slip process involving the Orowan loops. They are assumed to be transformed (probably during their

formation) into mobile prismatic loops by double cross slip. The derivation results in an equation in which the term $\gamma^{1/2}$ is replaced by $(\gamma^{1/2} - \gamma_0^{1/2})$, where γ_0 is another parameter usually small compared to γ.

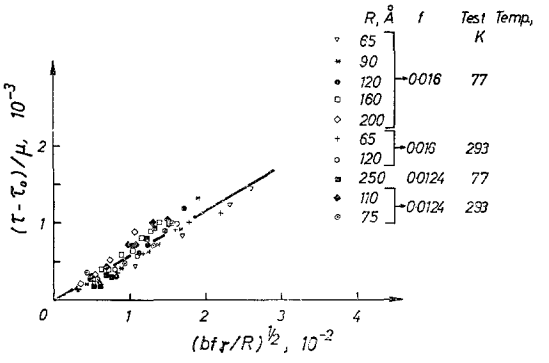

Figure 9 Comparison with the parabolic hardening law of Ashby.

In Fig. 9 representative data from the present experiments have been plotted as $(\tau - \tau_0)/\mu$ versus $(bf\gamma/R)^{1/2}$. These data can be represented adequately by a straight line with a slope between 0.05 and 0.1. These slopes are well below those observed experimentally for Cu–Al_2O_3 [24] ($c = 0.17$). It should be noted that Equation 9 can be applied only to particles with radii between about 70 and 200 Å, i.e. in the range where the particles are still coherent at the beginning of deformation. Below a radius of about 100 Å, another mechanism dominates whereby the observed parabolic behaviour has been explained by the softening of the crystal due to particle shearing [1, 13]. Therefore, it seems reasonable to suggest a similar mechanism for the crystals containing larger particles where the critical resolved shear stress is controlled by the Orowan mechanism. In this latter case, the relaxation of the stress concentration near the particle probably results from the Orowan loops being forced through the particles by the following dislocations which are emanating from the same source. If one assumes that some $\gamma_{\text{eff}} = k\gamma$ is the part of the shear strain which causes stress relaxation in the manner described by Ashby or Humphreys and Hirsch, the constant c' in Equation 9 is replaced by $c'^{1/2}$. Based on the experimental results, $k^{1/2} \simeq 0.4$, and, hence, $\gamma_{\text{eff}} \cong 0.17\,\gamma$. Perhaps the reduced value of θ_{II} of stage II strain hardening (Fig. 5) is also caused by particle shearing which effectively softens the crystal continuously. If this is true, the effect should be more pronounced for smaller particles, in agreement with the results shown in Fig. 5.

4. Conclusions

(1) The yield stress is controlled by particle shearing for particle radii less than 80 to 100 Å and by the Orowan mechanism for larger particles. The line tension responsible for the latter case is clearly dependent on the particle size as originally suggested by Ashby.

(2) The shape of the stress–strain curves varies systematically with the particle size. For radii below about 160 Å, the shape is parabolic with only a slight indication of a second work-hardening stage (II) before fracture. Above around 160 Å the three stage hardening behaviour becomes more pronounced which is more similar to that of pure copper, the principal difference being the decrease of the stage II hardening rate with decreasing precipitate size.

(3) The experimental data of the parabolic stress–strain stage can be fitted to either the Ashby or the Hirsch equations for parabolic work-hardening due to undeformable particles. However, the much lower work-hardening rates observed and the electron microscopic study suggest that the particles are sheared. This shearing process may occur by the initially formed Orowan rings being pushed through the particles by the stress fields of the following dislocations.

References

1. K. G. HARTMANN, *Z. Metallk.* **62** (1971) 736, 877.
2. K. MATSUNRA, M. TSUKAMOTO and K. WATANABE, *Acta Met.* **21** (1973) 1033.
3. S. D. LIVINGSTONE, *Trans. Met. Soc. AIME* **215** (1959) 566.
4. V. A. PHILLIPS, *Phil. Mag.* **11** (1965) 775.
5. H. GLEITER, *Acta Met.* **15** (1967) 1223.
6. M. F. ASHBY, *Phil. Mag.* **14** (1966) 1157.
7. M. H. LEWIS and J. W. MARTIN, *Acta Met.* **11** (1963) 1207.
8. P. B. HIRSCH and F. J. HUMPHREYS, *Proc. Roy. Soc.* **A318** (1970) 45, 73.
9. *Idem*, Proceedings of the Second International Conference on the Strength of Metals and Alloys (ASM, 1970) p. 545.
10. P. B. HIRSCH and F. J. HUMPHREYS, in "Physics of Strength and Plasticity", edited by A. S. Argon (MIT Press, Cambridge, Mass. 1969) p. 189.
11. D. DEW-HUGHES and W. D. ROBERTSON, *Acta Met.* **8** (1960) 147.
12. M. F. ASHBY, *Phil. Mag.* **21** (1970) 399.

13. K. HARTMANN and V. GEROLD, *Mat. Sci. Eng.* **10** (1972) 63.
14. V. A. PHILLIPS, *Trans. Met. Soc. AIME* **230** (1964) 967.
15. *Idem, Acta Met.* **14** (1966) 271.
16. V. A. PHILLIPS and S. D. LIVINGSTON, *Phil. Mag.* **7** (1962) 969.
17. F. J. HUMPHREYS, *Acta Met.* **16** (1968) 1069.
18. M. HANSEN, "Constitution of Binary Alloys" (McGraw-Hill, New York, Toronto, London, 1958) p. 470.
19. J. E. HILLIARD, *Trans. Met. Soc. AIME* **224** (1962) 906.
20. J. J. BECKER, *ibid* **209** (1957) 59.
21. L. M. BROWN and R. K. HAM, "Strengthening Methods in Crystals" edited by A. Kelley and R. B. Nicholson, Vol. 9 (Elsevier, Amsterdam, 1971) p. 53.
22. V. GEROLD and H. HABERKORN, *Phys. Stat. Sol.* **16** (1966) 675.
23. A. S. E. FORMAN and M. S. MAKIN, *Canad. J. Phys.* **45** (1967) 511.
24. R. EBELING and M. F. ASHBY, *Phil. Mag.* **13** (1966) 805.
25. M. F. ASHBY, in "Physics of Strength and Plasticity", edited by A. S. Argon (MIT Press, Cambridge, Mass. 1969).
26. M. WITT and V. GEROLD, *Scripta Met.* **3** (1969) 371.
27. M. F. ASHBY, in "Oxide Dispersion Strengthening", Proceedings of the Second Bolton Landing Conference, edited by G. S. Ansell, T. O. Cooper, and F. V. Lenel (Gordon and Breach, New York, London, Paris, 1968).
28. R. L. JONES and A. KELLY, *ibid.*
29. V. GEROLD, *Z. Metallk.* **62** (1971) 796.

Received 20 January and accepted 3 February 1975.